2013 IEEE/RSJ International Conference on
Intelligent Robots and Systems (IROS)
November 3-7, 2013. Tokyo, Japan

On the Geometric Phase Approach to Motion Planning for a Spherical Rolling Robot in Dynamic Formulation

Mikhail Svinin, Akihiro Morinaga, and Motoji Yamamoto

Abstract— **The paper deals with the problem of motion planning for a spherical rolling robot actuated by two internal rotors that are placed on orthogonal axes. To solve the problem, we employ the so-called geometric phase approach based on the fact that tracing a closed path in the space of input variables results in a non-closed path in the space of output variables. To set up the governing equations, the contact kinematic equations are modified by the condition of dynamic realizability, which constrains the component of the angular velocity of the rolling carrier and depends on the mass distribution, and parameterized. By using a motion planning strategy based on tracing two circles on the spherical surface, an exact and dynamically realizable motion planning algorithm is fabricated and verified under simulation.**

I. Introduction

The design and control of spherical rolling robots, that can be regarded as non-conventional vehicles, is still an insufficiently explored research area. Different schemes of spherical robots are reported in [1]–[6]. In this paper we consider a rolling robot actuated by two internal rotors.

One of the most important problems in the control of spherical robots is the construction of motion planning algorithms. In the majority of papers in the robotics literature this problem is considered for the so-called ball-plate system where the sphere is actuated by moving two parallel plates. Under such an actuation the spinning of the sphere around the vertical axis is canceled out and the sphere moves in the pure rolling mode. Typically, motion planning for the ball-plate system is conducted in kinematic formulation [7]–[11], and the extension of the proposed algorithms to different types of actuation is a challenging research problem.

It should be noted that if the number of actuators is more than two the motion planning can be decomposed and solved sequentially at the kinematic and dynamic levels. However, for the minimal number of actuators such a decomposition is impossible and the motion planning must be considered from the beginning in dynamic formulation.

The motion planning problem for the actuation by two rotors was first addressed in [2]. It was posed in the optimal control settings using an approximation by a Phillip Hall system [12]. However, since the robot dynamics are not nilpotent, this is not an exact representation of the system and it can result to inaccuracies. A motion planning strategy based on the iterative steering and nilpotent approximation is reported in [13]. An exact motion planning algorithm was described in [5], but the trajectories generated by this algorithm are not always dynamically realizable.

Since the mathematical model of rolling robot with two rotors is structurally similar to that for the ball-plate system, it is worthwhile to look at the two motion planning approaches developed for the kinematic model of pure rolling. The first is based on the optimal control theory [8], while the second deals with geometric phases [7], [12]. Numerical implementation of the optimal control approach, apart from the long computation time, can be sensitive to initial guess of the optimal controls. The geometric phase approach is based on the fact that a closed path in the space of the inputs variables results in a non-closed path in the space of the output variables. We resort to this approach to develop an exact motion planning algorithm, and this constitutes the main goal of this paper.

The paper is organized as follows. First, in Section II we review the mathematical model of the rolling robot and then, in Sections III, address the motion planning problem. There, by modifying the contact kinematic equations by the condition of dynamic realizability, we first establish a working model for solving the motion planning problem. Then, by using a motion planning strategy based on tracing spherical figure eights, we fabricate an exact and dynamically realizable motion planning algorithm and verify it under simulation. Finally, conclusions are drawn in Section IV.

II. Mathematical Model

Consider a rolling robot composed of a spherical shell (carrier) actuated by internal rotors. It is assumed that the rotors have the same mass distribution and the center of mass of the system is located at the geometric center. The rotors are mounted symmetrically along orthogonal axes as shown in Fig. 1. On each axis the two diametrically opposite rotors are actuated in tandem. This scheme, with actuation along two orthogonal axes, was first proposed in [2] and later on studied in [5].

Define the following coordinate frames (see Fig. 2): Σ_a is an inertial frame fixed in the contact plane, Σ_o is a frame fixed at the geometric center of the sphere. In addition, we introduce the contact frame of the object Σ_{co}, and the contact frame of the plane, Σ_{ca}. The contact coordinates are given by the angles u_o and v_o, describing the contact point on the sphere, and the displacements u_a and v_a, describing the contact point on the plane, and by the contact angle ψ which is defined as the angle between the x-axis of Σ_{co} and Σ_{ca}

M. Svinin is with International Research and Education Center, Faculty of Engineering, Kyushu University, 744 Motooka, Nishi-ku, Fukuoka 819-0395, Japan, svinin@mech.kyushu-u.ac.jp.

A. Morinaga and M. Yamamoto are with Mechanical Engineering Department, Kyushu University, 744 Motooka, Nishi-ku, Fukuoka 819-0395, Japan, morinaga@ctrl.mech.kyushu-u.ac.jp, and yamamoto@mech.kyushu-u.ac.jp.

978-1-4673-6357-0/13/$31.00 ©2013 IEEE

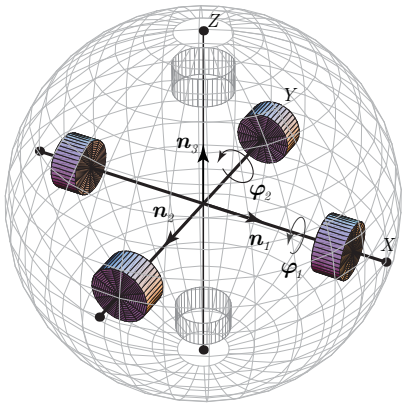

Fig. 1. Rolling system with orthogonal placement of rotors.

(the z-axes of these frames are aligned as depicted in Fig. 2). It is assumed that the frame Σ_{ca} is parallel to Σ_a, and in the zero configuration the axes of Σ_o are parallel to those of Σ_a.

The position of the contact point on the sphere is parameterized as

$$\boldsymbol{c}(u_o, v_o) = R \begin{bmatrix} -\sin u_o \cos v_o \\ \sin v_o \\ -\cos u_o \cos v_o \end{bmatrix}, \tag{1}$$

where R is the radius of the sphere. In this parameterization the origin is placed at the south pole of the sphere. In terms of the contact coordinates, the orientation matrix of the sphere (the orientation of Σ_o relative to Σ_a) is defined as

$$\boldsymbol{R} = \boldsymbol{R}_z^{\mathrm{T}}(\psi)\boldsymbol{R}_x^{\mathrm{T}}(v_o)\boldsymbol{R}_y^{\mathrm{T}}(u_o) = \begin{bmatrix} \boldsymbol{n}_1 & \boldsymbol{n}_2 & \boldsymbol{n}_3 \end{bmatrix}, \tag{2}$$

where $\boldsymbol{R}_x(v_o), \boldsymbol{R}_y(u_o)$, and $\boldsymbol{R}_z(\psi)$ are the matrices of elementary rotations, and the columns of the orientation matrix are defined as

$$\boldsymbol{n}_1 = \begin{bmatrix} \cos u_o \cos\psi + \sin u_o \sin v_o \sin\psi \\ -\cos u_o \sin\psi + \sin u_o \sin v_o \cos\psi \\ \cos u_o \cos v_o \end{bmatrix}, \tag{3}$$

$$\boldsymbol{n}_2 = \begin{bmatrix} \cos v_o \sin\psi \\ \cos v_o \cos\psi \\ -\sin v_o \end{bmatrix}, \tag{4}$$

$$\boldsymbol{n}_3 = \begin{bmatrix} -\sin u_o \cos\psi + \cos u_o \sin v_o \sin\psi \\ \sin u_o \sin\psi + \cos u_o \sin v_o \cos\psi \\ \cos u_o \cos v_o \end{bmatrix}. \tag{5}$$

Let $\boldsymbol{\omega}_o = \{\omega_x, \omega_y, \omega_z\}^{\mathrm{T}}$ be the angular velocity of the frame Σ_o, defined in projections onto the axes of Σ_a. The evolution of the contact coordinates can be constructed from the Montana equations [12] and represented as

$$\dot{u}_a = R\,\omega_y, \tag{6}$$
$$\dot{v}_a = -R\,\omega_x, \tag{7}$$
$$\dot{u}_o = -(\omega_x \sin\psi + \omega_y \cos\psi)/\cos v_o, \tag{8}$$
$$\dot{v}_o = -\omega_x \cos\psi + \omega_y \sin\psi, \tag{9}$$
$$\dot{\psi} = -\omega_z - (\omega_x \sin\psi + \omega_y \cos\psi)\tan v_o, \tag{10}$$

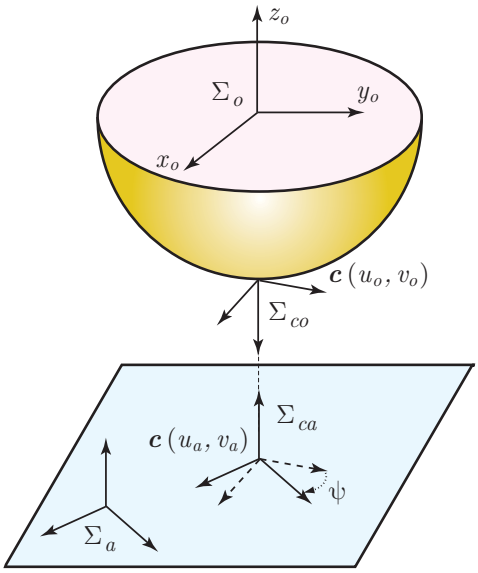

Fig. 2. Basic frames and contact coordinates.

The dynamic model for the system under consideration is established in [14]. Under the assumption that the motion does not start impulsively, the dynamic model admits the following integral [14]

$$\boldsymbol{J}_c\,\boldsymbol{\omega}_o + J_r \sum_{i=1}^{2} \boldsymbol{n}_i \dot{\varphi}_i = \boldsymbol{0}, \tag{11}$$

reflecting the conservation of the total angular momentum of the system about the contact point, which can be interpreted as the driving principle of the robot under consideration. Here, φ_i is the angle of rotation around the axis $\boldsymbol{n}_i$ J_r is the inertia moment of the single rotor around its axis of rotation, $\boldsymbol{J}_c = \mathrm{diag}\{J_{xx}, J_{xx}, J_{zz}\}$ is the inertia tensor of the composite system (rolling carrier and the rotors) with respect to the contact point, $J_{xx} = J_{zz} + MR^2$, $J_{zz} = \frac{2}{3}m_o R^2 + 2J_p + J_r$, M is the total mass of the system, m_o is the mass of the spherical shell, m_r is the mass of the single rotor and J_p is its inertia moment about the plane orthogonal to the axis of rotation.

III. Motion Planning

If the angular velocity $\boldsymbol{\omega}_o$ is given, one can define define the motion of the rotors by pre-multiplying (11) by the orthonormal vectors $\boldsymbol{n}_1$ and $\boldsymbol{n}_2$. For the kinematic motion to be dynamically feasible, one must have

$$\boldsymbol{n}_3 \cdot \boldsymbol{J}_c \boldsymbol{\omega}_o = 0. \tag{12}$$

This condition does not depend on the motion of rotors, and therefore can be called the condition of dynamic realizability. For the system under consideration the condition (12) can be written down as

$$k\,(n_{3x}\omega_x + n_{3y}\omega_y) + n_{3z}\omega_z = 0, \tag{13}$$

where n_{3x}, n_{3y}, n_{3z} are the components of the vector $\boldsymbol{n}_3$ given by (5), and the dimensionless constants $k = J_{xx}/J_{zz}$

is defined through the components of the inertia tensor $\boldsymbol{J}_c$:

$$k = 1 + \frac{MR^2}{\frac{2}{3}m_oR^2 + 2J_p + J_r}. \quad (14)$$

In general, the pure rolling motion ($\omega_z = 0$) is not realizable in the system with two rotors; it can be maintained only when $n_{3x}\omega_x + n_{3y}\omega_y = 0$. Hence, the conventional kinematics-based motion planning algorithms [7]–[11], designed for the model (6-10) under the assumption of pure rolling, are not directly applicable for the generation of dynamically realizable trajectories.

A. Parameterized form of the dynamically realizable contact kinematics

Note that the condition (12) imposes a constraint on the components of the vector $\boldsymbol{\omega}_o$, and this constraint needs to be embedded into the motion planning algorithms. If the motion planning is based on the direct specification of contact curves on the sphere, the embedding can be done as follows. Assume that the functions $u_o(t)$ and $v_o(t)$ are given. The kinematic equations (6-10) can now be casted as

$$\dot{u}_a = -R\cos\psi\cos v_o\,\dot{u}_o + R\sin\psi\,\dot{v}_o, \quad (15)$$

$$\dot{v}_a = R\sin\psi\cos v_o\,\dot{u}_o + R\cos\psi\,\dot{v}_o, \quad (16)$$

$$\dot{\psi} = -\omega_z + \sin v_o\,\dot{u}_o. \quad (17)$$

To guarantee the dynamic realizability, express ω_z in the last formula through ω_x and ω_y by using (13). In doing so, we first need to express ω_x, ω_y as well as n_{3x}, n_{3y}, n_{3z} in terms of the contact coordinates. From the definition of the angular velocity $\hat{\boldsymbol{\omega}}_o = \dot{\boldsymbol{R}}\boldsymbol{R}^{\mathrm{T}}$ [12], one obtains

$$\omega_x = -\dot{u}_o\cos v_o\sin\psi - \dot{v}_o\cos\psi, \quad (18)$$

$$\omega_y = -\dot{u}_o\cos v_o\cos\psi + \dot{v}_o\sin\psi, \quad (19)$$

Having expressed everything in terms of the contact coordinates, one can finally replace $\dot{\psi}$ in (17) by

$$\dot{\psi} = (1-k)\sin v_o\,\dot{u}_o + k\frac{\tan u_o}{\cos v_o}\dot{v}_o. \quad (20)$$

If we, formally, set here $k = 0$ the variable $\dot{\psi}$ will be defined as in the kinematic model with pure rolling. However, this case is purely hypothetical because by the definition (14) $k > 1$ always.

Assume that the position of the contact point on the sphere is parameterized by a spherical curve $\boldsymbol{c}(\theta) \triangleq \{x(\theta), y(\varphi), z(\theta)\}^{\mathrm{T}}$. Since the same point is defined by (1), one has

$$\boldsymbol{c}(u_o, v_o) = \boldsymbol{c}(\theta). \quad (21)$$

Differentiating this relationship, one obtains

$$\boldsymbol{c}_u\dot{u}_o + \boldsymbol{c}_v\dot{v}_o = \boldsymbol{c}_\theta\,\dot{\theta}, \quad (22)$$

where $\boldsymbol{c}_\theta \triangleq \partial\boldsymbol{c}/\partial\theta$, $\boldsymbol{c}_u \triangleq \partial\boldsymbol{c}/\partial u_o$ and $\boldsymbol{c}_v \triangleq \partial\boldsymbol{c}/\partial v_o$. The partial derivatives $\boldsymbol{c}_u$ and $\boldsymbol{c}_v$,

$$\boldsymbol{c}_u = R\begin{bmatrix} -\cos u_o\cos v_o \\ 0 \\ \sin u_o\cos v_o \end{bmatrix}, \quad \boldsymbol{c}_v = R\begin{bmatrix} \sin u_o\sin v_o \\ \cos v_o \\ \cos u_o\sin v_o \end{bmatrix}, \quad (23)$$

are defined from (1). To express $\boldsymbol{c}_u$ and $\boldsymbol{c}_v$ as functions of θ, one resolves (21) and obtains

$$\cos v_o = \sqrt{1-(y(\theta)/R)^2},\ \ \sin v_o = y(\theta)/R, \quad (24)$$

$$\cos u_o = \frac{-z(\theta)/R}{\sqrt{1-(y(\theta)/R)^2}},\ \sin u_o = \frac{-x(\theta)/R}{\sqrt{1-(y(\theta)/R)^2}}, \quad (25)$$

Therefore,

$$\boldsymbol{c}_u = \begin{bmatrix} z(\theta) \\ 0 \\ -x(\theta) \end{bmatrix},\ \boldsymbol{c}_v = \begin{bmatrix} -x(\theta)y(\theta)/\sqrt{R^2-y^2(\theta)} \\ \sqrt{R^2-y^2(\theta)} \\ -y(\theta)z(\theta)/\sqrt{R^2-y^2(\theta)} \end{bmatrix}, \quad (26)$$

Next, taking into account that the vectors $\boldsymbol{c}_u$ and $\boldsymbol{c}_v$ are orthogonal, one obtains from (22)

$$\dot{u}_o = \frac{1}{R^2\cos^2 v_o}\boldsymbol{c}_u^{\mathrm{T}}\boldsymbol{c}_\theta\,\dot{\theta}, \quad \dot{v}_o = \frac{1}{R^2}\boldsymbol{c}_v^{\mathrm{T}}\boldsymbol{c}_\theta\,\dot{\theta}, \quad (27)$$

and substituting (27) into (15-17) yields the following system of differential equations

$$u_a'(\theta) = -\frac{\cos\psi(\varphi)}{\sqrt{R^2-y^2(\varphi)}}\boldsymbol{c}_u^{\mathrm{T}}\boldsymbol{c}_\theta + \frac{\sin\psi(\theta)}{R}\boldsymbol{c}_v^{\mathrm{T}}\boldsymbol{c}_\theta, \quad (28)$$

$$v_a'(\theta) = \frac{\sin\psi(\theta)}{\sqrt{R^2-y^2(\theta)}}\boldsymbol{c}_u^{\mathrm{T}}\boldsymbol{c}_\theta + \frac{\cos\psi(\theta)}{R}\boldsymbol{c}_v^{\mathrm{T}}\boldsymbol{c}_\theta, \quad (29)$$

$$\psi'(\theta) = \left\{\frac{(1-k)y(\theta)\boldsymbol{c}_u^{\mathrm{T}}}{(R^2-y^2(\theta))} + \frac{kx(\theta)\boldsymbol{c}_v^{\mathrm{T}}}{z(\theta)\sqrt{R^2-y^2(\theta)}}\right\}\frac{\boldsymbol{c}_\theta}{R} \quad (30)$$

describing the change of the contact coordinates as function of θ. Here, primes denote the partial differentiation with respect to the variable θ, while dots are reserved for the time differentiation.

B. Motion planning strategy

Define $\boldsymbol{c}(\theta)$ to be a periodic curve, $\boldsymbol{c}(\theta) = \boldsymbol{c}(\theta \pm 2k\pi)$, $k \in \mathbb{Z}$, such that $\boldsymbol{c}(0) = \{0, 0, -R\}^{\mathrm{T}}$ and therefore $u_o(2\pi n) = v_o(2\pi n) = 0$, i.e. the values of u_o and v_o in the initial and final configurations are assumed to be zero. The assumption restricts the generality of the problem statement. However, the movement to be found under this assumption can be thought of as a non-trivial maneuver of a general reconfiguration strategy similar to that considered in [7], [9], [10]. The generality can be easily restored if the non-trivial maneuver is accompanied by a trivial one (bringing u_o and v_o to the desired values).

To satisfy the boundary conditions $u_a(2\pi n) = u_{a,\mathrm{des}}$, $v_a(2\pi n) = v_{a,\mathrm{des}}$, $\psi(2\pi n) = \psi_{\mathrm{des}}$, for a given the number of steps n, there must be at least three free parameters in a specific representation of the curve $\boldsymbol{c}(\theta)$. The three parameters can be introduced as follows. Let $\boldsymbol{c}(\theta)$ be a spherical figure eight with characteristic sizes of its leaves a and b. The orientation of this curve on the sphere is defined up to the angle γ of rotation around the axis OZ of the frame Σ_o. The motion planning problem is then reduced to the following formulation. Given a spherical figure eight

$$\boldsymbol{c}(\theta) = \boldsymbol{R}_z(\gamma)\bar{\boldsymbol{c}}(a, b, \theta), \quad (31)$$

where $\boldsymbol{R}_z(\gamma)$ is the matrix of rotation around the axis OZ, find the parameters a, b, and γ so that tracing this curve n times brings the system to the desired configuration.

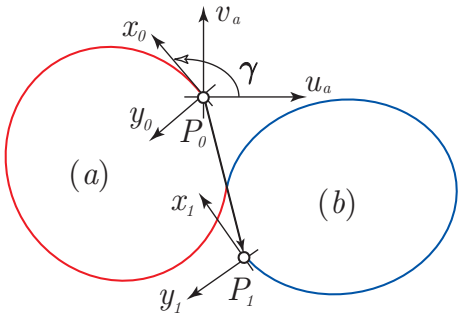

Fig. 3. One-step movement in the contact plane. The 1st half-step (tracing the 1st leaf of the figure eight) is shown in red, while the 2nd in blue color. Also shown are the initial orientation and the assignment of local frames.

If the spherical figure eight is traced one time, the contact point in the contact plane is shifted from P_0 to P_1 as shown schematically in Fig. 3. The length of the linear displacement $h = |\overrightarrow{P_0P_1}|$ defines the non-holonomic shift. It is assumed that the x-axes of the local frames associated with the movement steps are oriented along the tangent vectors to the contact curve in the contact plane as shown in Fig. 3. The orientation of the frame $P_1x_1y_1$ with respect to $P_0x_0y_0$ defines the holonomy angle η.

The non-holonomic shift h and the holonomy angle η are the same for all the movement steps. They are functions of the generalized parameters a and b and do not depend on the angle γ. To compute $h(a,b)$ and $\eta(a,b)$, one can set in (31) $\gamma = 0$ and integrate the system (28-30) numerically for one step of movement ($\theta \in [0, 2\pi]$) with zero initial conditions. This defines $h(a,b) \triangleq \sqrt{\bar{u}_a^2(2\pi) + \bar{v}_a^2(2\pi)}$ and $\eta(a,b) \triangleq \bar{\psi}(2\pi)$. Here, we the bar denotes the contact coordinates obtained for $\gamma = 0$.

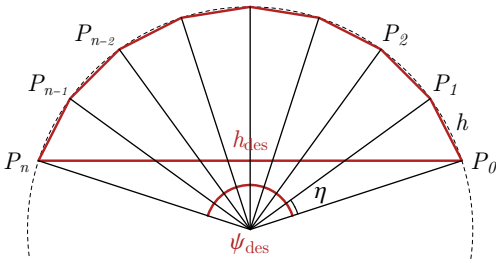

Fig. 4. The change of the vectors of the non-holonomic shift during n-step movement.

Having formally defined the functions $h(a,b)$ and $\eta(a,b)$, one can establish their relation with $h_{\text{des}} = \sqrt{u_{a,\text{des}}^2 + v_{a,\text{des}}^2}$ and ψ_{des}. As one traces the spherical figure eight n times, the vector of the non-holonomic shift will rotate each time by the angle η as shown in Fig. 4. Therefore, the points $P_0, P_1, \ldots, P_n$ will lie on a circle of (now unknown) radius r. Clearly,

$$\eta(a,b) = \psi_{\text{des}}/n. \tag{32}$$

The formula for $h(a,b)$ can be established as follows. From the relation between the length of the chord of a circular arc and the corresponding central angle one has $h(a,b) = 2r\sin(\eta(a,b)/2)$, and $h_{\text{des}} = 2r\sin(n\,\eta(a,b)/2)$, where r is the radius of the circular arc. By excluding it, one obtains

$$h(a,b) = \frac{\sin(\eta(a,b)/2)}{\sin(n\,\eta(a,b)/2)} h_{\text{des}} = \frac{\sin(\psi_{\text{des}}/2n)}{\sin(\psi_{\text{des}}/2)} h_{\text{des}}. \tag{33}$$

Note that if $\psi_{\text{des}} = 0$ the leaves of the figure eight have the same size, $a = b$, and by evaluating the indeterminacy in (33) one obtains

$$h(a,a) = h_{\text{des}}/n. \tag{34}$$

In general, one determines the parameters a and b from solving the system (32,33), which can be done by iterating the nonlinear system (32,33) with numerical integration of the system (28-30) on each iteration step. Having established a and b, one can finally establish the orientation of the frame $P_0x_0y_0$ with respect to the frame Σ_a, denoted by the angle γ, from the requirement that the vector of the resulting displacement $\overrightarrow{P_0P_n}$ points to the desired destination (see [15] for the details).

C. Case study

To specify the curve $\bar{\boldsymbol{c}}(\theta)$ in a relatively simple analytical way, one can concatenate spherical polygons (geodesic triangles [16] or quadrilaterals [17]) or circles [11], or use the generalized Viviani curve [15].

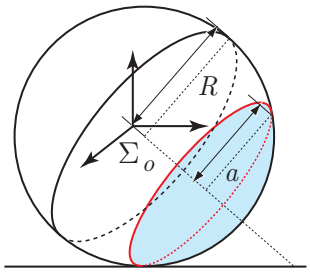

Fig. 5. Spherical circle

In this case study we would like to clarify the formation and the dependance of the non-holonomic shift on the inertia distribution specified by the parameters k. For this purpose it will suffice to deal with symmetric figures eights ($a = b$). Consider a maneuver when one traces a circle of radius a on the spherical surface as shown in Fig. 5. The curve $\bar{\boldsymbol{c}}(a,\theta)$ in (31) is specified as

$$\bar{\boldsymbol{c}}(a,\theta) = \begin{bmatrix} a\sin\theta \\ -a\cos\alpha\cos\theta + d\sin\alpha \\ -a\sin\alpha\cos\theta - d\cos\alpha \end{bmatrix}, \tag{35}$$

where $d = R\sqrt{1-(a/R)^2}$, $\sin\alpha = a/R$ and $\cos\alpha = d/R$. By concatenating two circles, one defines a spherical figure eight.

Assume that the number of movement steps $n = 1$. Consider first the case of pure rolling ($k = 0$). The trajectory of the contact point on the contact plane is composed of two

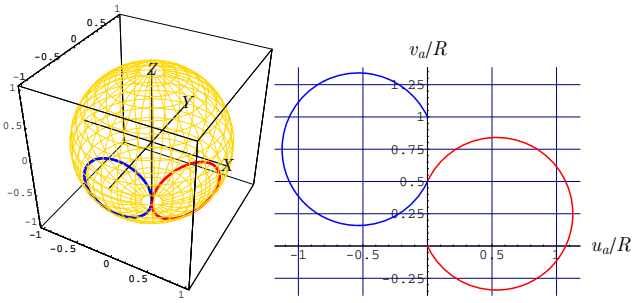

Fig. 6. Contact point trajectory for $k = 0$ and $a \approx 0.533681R$.

circular segments. The normalized non-holonomic shift at the end of movement can be defined analytically [11] as

$$h/R = 4\frac{a/R}{\sqrt{1-(a/R)^2}}\sin\left(\pi\sqrt{1-(a/R)^2}\right). \qquad (36)$$

In the simulation we set $a \approx 0.533681R$ so that $h/R = 1$. The orientation of the figure eight on the sphere, defined by the angle γ of rotation around the axis OZ of the frame Σ_o, is set as $\gamma \approx -1.13393$rad so that the sphere propels along the v_a axis of the frame Σ_a. The simulation results for the case of pure rolling ($k = 0$) are shown in Fig. 6.

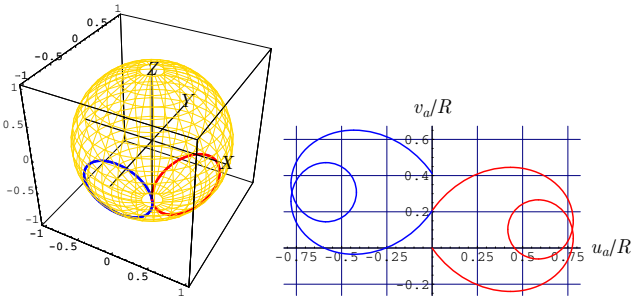

Fig. 7. Contact point trajectory for $k = 2.5$ and $a \approx 0.533681R$.

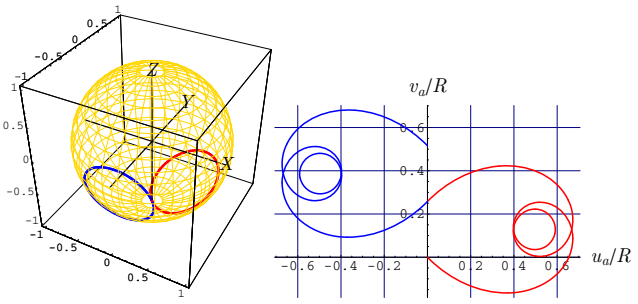

Fig. 8. Contact point trajectory for $k = 5$ and $a \approx 0.533681R$.

Next, we inspect the contact point trajectories obtained with the same radius a of the spherical circle but with different inertia ratio k. The simulation results corresponding to $k = 2.5$ and $k = 5$ are shown in Fig. 7 and Fig. 8. Here, for the same a we have different non-holonomic shifts: $h \approx 0.410842R$ for $k = 2.5$ and $h \approx 0.515783R$ for $k = 5$.

To direct the resulting displacement along the v_a axis, one sets $\gamma \approx -0.965672$rad for $k = 2.5$ and $\gamma \approx -0.797416$rad for $k = 5$. One can see that, while the length of the of the trajectory of the contact point in the contact plane is exactly the same as that obtained for the case of pure rolling (kinematic model), its form is drastically different. In particular, one can see that the number of internal loops in the contact plane is increasing with the increase of k.

The normalized non-holonomic shift is plotted in Fig. 9 as a function of k for $a \approx 0.533681R$. Here, one can observe the existence of the inertia ratios ($k_1 \approx 0.233154$, $k_2 \approx 2.64357$, $k_3 \approx 5.20728$, $k_4 \approx 7.80506$, $k_5 \approx 10.9801, \ldots$) producing the zero resulting displacement. One can say that for the given a/R at the zeros of h/R the system behavior is that of a holonomic one. It is also interesting to note that the number of self-intersections of the trajectory of the contact point on the plane for the half step of movement is exactly i if $k \in [k_i, k_{i+1}]$, $i = 0, 1, 2, \ldots$. This statement was verified under simulations.

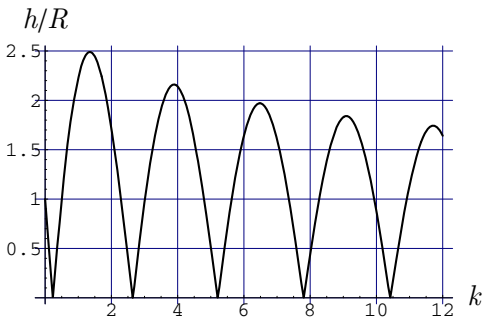

Fig. 9. Non-holonomic shift as a function of k for $a \approx 0.533681R$.

In the final series of simulations we assume that the inertia ratio k is given. To produce a desired non-holonomic shift, one needs to re-size the spherical figure eight and redefine its orientation on the sphere. Let us set the inertia ratio as $k = 2.5$. The normalized non-holonomic shift is plotted in Fig. 10 as a function of a/R for the given k. Assume now that the desired value for the non-holonomic shift is $h/R = 1$ (that is as in the pure rolling case). For the given h/R we have a multiplicity of solutions: $a_1 = 0.300429R$, $a_2 = 0.491471R$, $a_3 = 0.538682R$, $a_4 = 0.609147R, \ldots$.

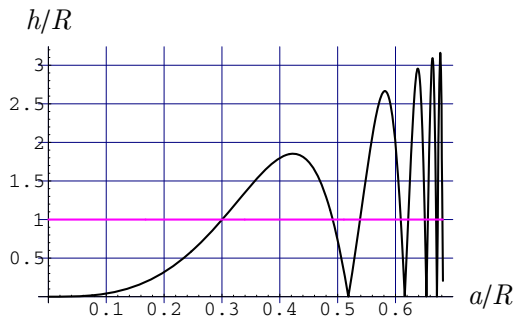

Fig. 10. Non-holonomic shift as a function of a/R for $k = 2.5$.

To align the resulting displacement along the v_a axis, we set $\gamma \approx 0.931883$rad for $a \approx 0.300429R$, and $\gamma \approx -0.69726$rad for $a \approx 0.491471R$. The trajectories of the contact point on the sphere and on the plane corresponding to the first two solutions obtained are shown in Fig. 11 and Fig. 12. It is clear that the first solution produces the contact point trajectory of minimal (compare to the other solutions) length. It is also interesting to note that the length of the contact point trajectory for first solution is considerably smaller than that corresponding to the kinematic model of pure rolling. This shows the effect of the spinning motion when it is not canceled out but dynamically constrained.

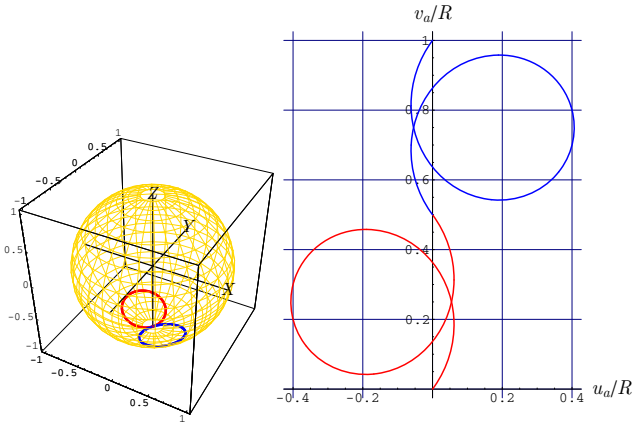

Fig. 11. Contact point trajectory for $k = 2.5$ and $a \approx 0.300429R$.

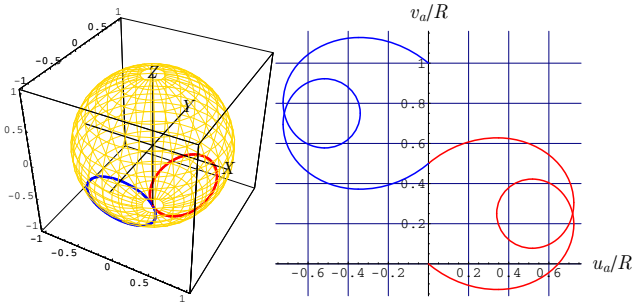

Fig. 12. Contact point trajectory for $k = 2.5$ and $a \approx 0.491471R$.

IV. Conclusions

An analysis of the motion planning problem for a spherical rolling robot, actuated by two internal rotors that are placed on orthogonal axes has been undertaken in this paper. A mathematical model for solving the motion planning problem has been obtained by modifying the contact kinematic equations by the condition of dynamic realizability which constrains the component of the angular velocity of the rolling carrier. By using a motion planning strategy based on tracing a spherical figure eight, an exact and dynamically realizable motion planning algorithm has been fabricated and verified under simulation. The dependence of the resulting non-holonomic shift on the mass distribution was clarified. It has been shown that for the same tracing figures the dynamically realizable trajectories on the contact plane are essentially different from and more complex than those obtained with the use of the kinematic model of pure rolling. Also, the dynamically realizable contact paths are shorter than their kinematic counterparts. This can be explained by the contribution of the spinning motion, which is not completely canceled but only dynamically constrained.

References

[1] A. Bicchi, A. Balluchi, D. Prattichizzo, and A. Gorelli, "Introducing the "Sphericle": an experimental testbed for research and teaching in nonholonomy," in *Proc. IEEE Int. Conference on Robotics and Automation*, vol. 3, Albuquerque, New Mexico, April 21–27 1997, pp. 2620–2625.

[2] S. Bhattacharya and S. Agrawal, "Spherical rolling robot: A design and motion planning studies," *IEEE Transactions on Robotics and Automation*, vol. 16, no. 6, pp. 835–839, December 2000.

[3] A. Javadi and P. Mojabi, "Introducing Glory: A novel strategy for an omnidirectional spherical rolling robot," *ASME Journal of Dynamic Systems, Measurement, and Control*, vol. 126, no. 3, pp. 678–683, September 2004.

[4] M. Ishikawa, Y. Kobayashi, R. Kitayoshi, and T. Sugie, "The surface walker: a hemispherical mobile robot with rolling contact constraints," in *Proc. IEEE/RSJ Int. Conference on Intelligent Robots and Systems, IROS'2009*, St. Louis, USA, October 10–15 2009, pp. 2446–2451.

[5] V. Joshi and R. Banavar, "Motion analysis of a spherical mobile robot," *Robotica*, vol. 27, no. 3, pp. 343–353, May 2009.

[6] A. Borisov, A. Kilin, and I. Mamaev, "How to control Chaplygin's sphere using rotors. Part II," *Regular and Chaotic Dynamics*, vol. 18, no. 1–2, pp. 144–158, 2013.

[7] Z. Li and J. Canny, "Motion of two rigid bodies with rolling constraint," *IEEE Trans. on Robotics and Automation*, vol. 6, no. 1, pp. 62–72, 1990.

[8] V. Jurdjevic, "The geometry of the plate-ball problem," *Archive for Rational Mechanics and Analysis*, vol. 124, no. 4, pp. 305–328, December 1993.

[9] A. Marigo and A. Bicchi, "Rolling bodies with regular surface: Controllability theory and applications," *IEEE Trans. on Automatic Control*, vol. 45, no. 9, pp. 1586–1599, September 2000.

[10] R. Mukherjee, M. Minor, and J. Pukrushpan, "Motion planning for a spherical mobile robot: Revisiting the classical ball-plate problem," *ASME Journal of Dynamic Systems, Measurement and Control*, vol. 124, no. 4, pp. 502–511, 2002.

[11] M. Svinin and S. Hosoe, "Motion planning algorithms for a rolling sphere with limited contact area," *IEEE Transactions on Robotics*, vol. 24, no. 3, pp. 612–625, June 2008.

[12] R. Murray, Z. Li, and S. Sastry, *A Mathematical Introduction to Robotic Manipulation*. Boca Raton: CRC Press, 1994.

[13] A. Morinaga, M. Svinin, and M. Yamamoto, "On the motion planning problem for a spherical rolling robot driven by two rotors," in *Proc. IEEE/SICE Int. Symposium on System Integration*, Fukuoka, Japan, December 16–18 2012, pp. 704–709.

[14] M. Svinin, A. Morinaga, and M. Yamamoto, "On the dynamic model and motion planning for a spherical rolling robot actuated by orthogonal internal rotors," *Regular and Chaotic Dynamics*, vol. 18, no. 1–2, pp. 126–143, 2013.

[15] M. Svinin and S. Hosoe, "Planning of smooth motions for a ball-plate system with limited contact area," in *Proc. IEEE Int. Conference on Robotics and Automation*, vol. 1, Pasadena, CA, May 19-23 2008, pp. 1193–1200.

[16] K. Harada, T. Kawashima, and M. Kaneko, "Rolling based manipulation under neighborhood equilibrium," *The International Journal of Robotics Research*, vol. 21, no. 5-6, pp. 463–474, 2002.

[17] A. Bicchi and A. Marigo, "Dexterous grippers: Putting nonholonomy to work for fine manipulation," *The International Journal of Robotics Research*, vol. 21, no. 5-6, pp. 427–442, May-June 2002.